Nitric Oxide-Induced Formation of the S_{-2} State in the Oxygen-Evolving Complex of Photosystem II from *Synechococcus elongatus*†

Josephine Sarrou,*,‡,§ Sabina Isgandarova,§ Jan Kern,§ Athina Zouni,§ Gernot Renger,§ Wolfgang Lubitz,‡ and Johannes Messinger‡,§

Max-Planck-Institut für Strahlenchemie, Stiftstrasse 34-36, D-45470 Mülheim an der Ruhr, Germany, and Max-Volmer-Laboratorium der TU Berlin, Strasse des 17 Juni 135, D-10623 Berlin, Germany

Received June 19, 2002; Revised Manuscript Received November 26, 2002

ABSTRACT: In spinach photosystem II (PSII) membranes, the tetranuclear manganese cluster of the oxygen-evolving complex (OEC) can be reduced by incubation with nitric oxide at −30 °C to a state which is characterized by an Mn_2(II, III) EPR multiline signal [Sarrou, J., Ioannidis, N., Deligiannakis, Y., and Petrouleas, V. (1998) *Biochemistry 37*, 3581−3587]. This state was recently assigned to the S_{-2} state of the OEC [Schansker, G., Goussias, C., Petrouleas, V., and Rutherford, A. W. (2002) *Biochemistry 41*, 3057−3064]. On the basis of EPR spectroscopy and flash-induced oxygen evolution patterns, we show that a similar reduction process takes place in PSII samples of the thermophilic cyanobacterium *Synechococcus elongatus* at both −30 and 0 °C. An EPR multiline signal, very similar but not identical to that of the S_{-2} state in spinach, was obtained with monomeric and dimeric PSII core complexes from *S. elongatus* only after incubation at −30 °C. The assignment of this EPR multiline signal to the S_{-2} state is corroborated by measurements of flash-induced oxygen evolution patterns and detailed fits using extended Kok models. The small reproducible shifts of several low-field peak positions of the S_{-2} EPR multiline signal in *S. elongatus* compared to spinach suggest that slight differences in the coordination geometry and/or the ligands of the manganese cluster exist between thermophilic cyanobacteria and higher plants.

Photosynthetic water oxidation is catalyzed by the tetranuclear manganese cluster (Mn_4 cluster) of the oxygen-evolving complex (OEC)[1] in photosystem II (PSII) (for reviews, see refs *1*−*3*). On the basis of the Kok model (*4*), the OEC undergoes four one-electron oxidation state transitions during the sequential absorption of photons by PSII: $S_0 \rightarrow S_1$, ..., $S_3 \rightarrow S_4$. O_2 is released during the $S_4 \rightarrow S_0$ transition. After prolonged dark adaptation, the complex is found in the S_1 state. To explain the mixing of S states during a flash train, which is evident from the damping of the period four oscillation of flash-induced oxygen yields, Kok and co-workers postulated that a miss (α) and a double-hit (β) probability is coupled with each flash-induced S state transition (*4*).

EPR spectroscopy has been instrumental in characterizing the S states. At liquid helium temperatures, both the S_2 and S_0 states give rise to a ground state $S = {}^1/_2$ EPR multiline signal centered at $g \approx 2$ (*5*−*8*). From the S_2 state also other spectroscopic forms exist which are characterized by signals at $g = 4.1$ (*9*, *10*) or $g = 6$ and $g = 10$ (*11*). The S_1 state is only EPR detectable using parallel mode microwave excitation. A broad $g = 4.8$ signal (*12*, *13*) and a $g = 12$ multiline signal (*14*) have been reported. From the S_3 state, low-field EPR peaks at $g = 6.7$ and 8−12 have been measured in perpendicular and parallel mode EPR, respectively (*15*−*17*). Together with information from other techniques, these EPR results show that the Mn_4 cluster is oxidized during the $S_0 \rightarrow S_1$ and $S_1 \rightarrow S_2$ transitions. Whether a Mn-centered or ligand-centered oxidation takes place during the $S_2 \rightarrow S_3$ transition is still under debate (*18*, *19*).

In addition to the normal S states of the Kok cycle, the OEC can attain redox states below S_0. These states can be obtained by incubation of PSII samples with small hydrophilic reductants such as NH_2OH, N_2H_4, or H_2O_2 (*20*−*22*) or with redox-active gases such as H_2S (*23*) or $NO^{\bullet}$ (*24*−*26*). A detailed analysis of flash-induced oxygen evolution patterns has revealed that a rather stable and selective population of S states down to the S_{-3} state is possible (*27*). Recently, first indications for the S_{-4} and S_{-5} states have been reported (*28*). The existence of these reduced states and their stability down to the S_{-3} state are in line with the

† Financial support by the Deutsche Forschungsgemeinschaft (Sfb 498, TP C3, C4, C5, and Me 1629/2-2), by TMR (FMRX-CT98-0214), and by the MPG is gratefully acknowledged.

* To whom correspondence should be addressed. E-mail: sarrou@mpi-muelheim.mpg.de. Telephone: +49 208 306 3865. Fax: +49 208 306 3951. Present address: Department of Chemistry, University of California, Davis, CA 95616 (e-mail, isarrou@ucdavis.edu).

‡ Max-Planck-Institut für Strahlenchemie.

§ Max-Volmer-Laboratorium der TU Berlin.

[1] Abbreviations: α and β, miss and double-hit probabilities during flash-induced oxygen evolution, respectively; α_{Y_D-NO}, miss factor for proposed direct oxidation of Y_D-NO by $P680^+$; chl, chlorophyll; cyt, cytochrome; DCMU, 3-(3,4-dichlorophenyl)-1,1-dimethylurea; DMSO, dimethyl sulfoxide; EPR, electron paramagnetic resonance; EXAFS, extended X-ray absorption fine structure; MES, 2-(*N*-morpholino)-ethanesulfonic acid; OEC, oxygen-evolving complex; PSII, photosystem II; PSIIcc, PSII core complexes; S states, S_{-5}−S_4 oxidation states of the OEC; Y_D, redox active tyrosine 160 of the D2 polypeptide of PSII; Y_Z, redox active tyrosine 161 of the D1 polypeptide of PSII; Y_D-NO, nitrosotyrosine D.

10.1021/bi026327p CCC: $25.00
Published on Web 01/07/2003

assignment of the dark-stable S_1 state to $Mn_4(III_2, IV_2)$ (*19*) (see, however, ref *29*).

In spinach PSII membranes, the reduction of the Mn_4 cluster with NO• at −30 °C leads to the formation of an intense EPR multiline signal which was recently assigned to the S_{-2} state (*30*). The S_{-2} EPR multiline signal can be very well simulated by a magnetically isolated $S = {}^1/_2$ Mn_2-(II, III) dimer (*25*). For unknown reasons, the other two Mn ions of the OEC do not contribute to this signal, but on the basis of the above assignment for the S_1 state, the redox states of the whole cluster should be Mn_4(II, III, III, III) in the S_{-2} state.

In light of the emerging details about the structure of PSII in the thermophilic cyanobacterium *Synechococcus elongatus* based on X-ray crystallography (*31*, *32*) and the lack of crystallographic data about the otherwise better studied PSII from higher plants (*33*−*36*), it is interesting to compare the structure and function of the two systems in detail. In this regard, EPR measurements can play an important role because magnetic couplings are sensitive to changes in the structure and ligands of the OEC. The S_0, S_2, and S_3 state EPR signals have been detected in samples from both organisms and show only minor differences (*17*, *37*, *38*). This is in agreement with structural information from EXAFS measurements on the S_1 and S_2 states (*37*). Similarly, kinetic studies on the temperature dependence of the individual S state oxidations led to the conclusion that the reaction coordinates are very similar in cyanobacteria and plants (*39*, *40*). In terms of EPR spectroscopy, a notable exception is the $g = 4.1$ signal of the S_2 state. Despite intense efforts, this EPR signal has not been detected in *S. elongatus* samples (*41*).

In this study, we analyze the reactivity of NO• with the OEC in spinach and *S. elongatus* samples employing flash-induced oxygen evolution measurements and CW EPR spectroscopy. On the basis of the presented data and the results from the literature, the close overall similarities of the OEC in cyanobacteria and higher plants are discussed together with possible structures of the Mn_4 cluster in the S_{-2} state.

MATERIALS AND METHODS

Sample Preparation. The thermophilic cyanobacterium *S. elongatus* was grown, and thylakoid membranes were prepared as described in ref *42* with some modifications. PSII core complexes (PSIIcc) were extracted from the membranes using β-dodecyl maltoside as a detergent and purified by weak anion exchange chromatography as described previously (*43*). Monomeric and dimeric PSIIcc were separated chromatographically (details will be published elsewhere). Both forms of the PSIIcc are fully active in water oxidation and show the same subunit composition as tested by MALDI-TOF mass spectrometry and SDS gel electrophoresis. The dimeric PSIIcc are similar to the material used to grow single crystals that are suitable for X-ray structure analysis (*31*). For comparison, PSII membranes were isolated from market spinach by standard procedures (*44*, *45*).

NO• Incubation. For NO• incubation, all samples were transferred into buffer A [0.4 M sucrose, 15 mM NaCl, 5 mM $MgCl_2$, and 40 mM MES (pH 6.5)]. The final chlorophyll concentrations were 4−5, 0.8, and 5−6 mg/mL for *S. elongatus* PSIIcc, *S. elongatus* thylakoids, and spinach PSII membranes, respectively. To test the effect of cryoprotectants on the NO• reduction, the sucrose in buffer A was substituted with either 25% glycerol or 400 mM mannitol. In the case of D_2O samples, buffer A was prepared with D_2O (99.9%, euriso-top) and the samples were washed twice with D_2O buffer, then incubated for 3 h on ice, and finally washed once more in D_2O buffer.

NO• treatment was carried out anaerobically in dim green light at 0 °C in 4 mm EPR quartz tubes by slowly bubbling NO• through the samples. This procedure took ∼1 min, and the final NO• concentrations in the samples was estimated on the basis of the known solubility of NO• in water (3 mM at 0 °C) to be 0.2 and 0.6 mM for *S. elongatus* and spinach, respectively. The EPR tubes were then immediately sealed and transferred into liquid nitrogen. This was followed by an overnight incubation in a freezer at −30 ± 2 °C.

EPR. CW EPR spectra were recorded at liquid helium temperatures on a Bruker ESP 300E instrument fitted with a liquid helium cryostat (Oxford ESR 9) and a standard Bruker TE102 cavity.

Flash-Induced Oxygen Evolution Patterns. Flash-induced oxygen evolution patterns of *S. elongatus* thylakoids and PSII membranes were obtained in the absence of exogenous electron acceptors with a home-built Joliot type (bare platinum) electrode (*46*, *47*) at 20 °C. Saturating flashes at a frequency of 2 Hz were provided through a fiber optic by a xenon flash lamp (EG&G, model PS 302, light pack FY-604). For the oxygen measurements, the NO•-treated samples were transferred, in the dark, from liquid nitrogen to ice temperatures. To reduce the NO• concentration in the samples to levels that cannot be detected by EPR (data not shown), the space in the EPR tubes above the samples was carefully flushed with nitrogen while the sample was still frozen. After thawing had been completed, the samples were then slowly bubbled with 1 mL of nitrogen using a syringe and finally transferred into Eppendorf reaction vials. They were kept anaerobically on ice until shortly before the oxygen measurements, for which they were diluted in buffer A to chlorophyll concentrations of 0.2 and 1 mg/mL for *S. elongatus* thylakoids and spinach PSII membranes, respectively.

Extended Kok Model. The data were analyzed using a spreadsheet program with a minimization routine. Our extended Kok model assumes, like the original one (*4*), equal miss and double-hit probabilities for all S state transitions. This is an approximation, because these transition probabilities depend on the redox equilibria between the different cofactors of PSII, which are likely to be S state-dependent (see ref *56*). However, unequal misses cannot be used, because no reliable information exists at present about the magnitude of this S state dependence. It is also noteworthy that in the past very reliable results have been obtained with the equal misses approximation. The extended Kok model used in this study also includes, in addition to the normal S states that are populated during oxygen evolution (S_0−S_3), the S_{-5}−S_{-1} states. PSII can be found in these redox states after reduction with exogenous electron donors or during photoactivation (*27*, *48*). We like to point out that the inclusion of the S_{-4} and S_{-5} states (only used in fit NO5) is speculative at this point and that further evidence is required to prove their existence. Within this model, the S state

populations ([S_i], $i = -5$ to 3) after the nth flash are given by

$$\begin{bmatrix}[S_{-5}]_n\\ [S_{-4}]_n\\ [S_{-3}]_n\\ [S_{-2}]_n\\ [S_{-1}]_n\\ [S_0]_n\\ [S_1]_n\\ [S_2]_n\\ [S_3]_n\end{bmatrix} = \begin{bmatrix}\alpha & 0 & 0 & 0 & 0 & 0 & 0 & 0 & 0\\ \gamma & \alpha & 0 & 0 & 0 & 0 & 0 & 0 & 0\\ \beta & \gamma & \alpha & 0 & 0 & 0 & 0 & 0 & 0\\ 0 & \beta & \gamma & \alpha & 0 & 0 & 0 & 0 & 0\\ 0 & 0 & \beta & \gamma & \alpha & 0 & 0 & 0 & 0\\ 0 & 0 & 0 & \beta & \gamma & \alpha & 0 & \beta & \gamma\\ 0 & 0 & 0 & 0 & \beta & \gamma & \alpha & 0 & \beta\\ 0 & 0 & 0 & 0 & 0 & \beta & \gamma & \alpha & 0\\ 0 & 0 & 0 & 0 & 0 & 0 & \beta & \gamma & \alpha\end{bmatrix} \cdot \begin{bmatrix}[S_{-5}]_{n-1}\\ [S_{-4}]_{n-1}\\ [S_{-3}]_{n-1}\\ [S_{-2}]_{n-1}\\ [S_{-1}]_{n-1}\\ [S_0]_{n-1}\\ [S_1]_{n-1}\\ [S_2]_{n-1}\\ [S_3]_{n-1}\end{bmatrix} \cdot d \quad (1)$$

where γ is the single-hit probability ($\gamma = 1 - \alpha - \beta$) and d an activity parameter that compensates for changes in the number of active PSII centers during the flash train (*27*). The oxygen yield of the nth flash, Y_n^{fit}, is calculated by

$$Y_n^{\text{fit}} = (1 - \alpha)[S_3]_{n-1} + \beta[S_2]_{n-1} \quad (2)$$

The program is minimizing the expression

$$dy_n^2 = \sum_{n=1}^{F}[Y_n^{\text{exp}} - Y_n^{\text{fit}}(\sum_{n=1}^{F} Y_n^{\text{exp}}/\sum_{n=1}^{F} Y_n^{\text{fit}})]^2 \quad (3)$$

by varying the parameters indicated in the tables (negative values were not permitted). In eq 3, Y_n^{exp} is the relative oxygen yield of the nth flash and F equals the number of analyzed flashes ($F = 16$ for this study). The normalization criterion is given by

$$\sum_{i=-5}^{3}[S_i] = 1 \quad (4)$$

The fit quality is calculated according to eq 5

$$\text{fq} = \frac{dy_n^2}{F - P} \quad (5)$$

where P is the number of free parameters in the fit.

RESULTS

EPR. Figure 1A shows an EPR difference spectrum (the NO•-incubated state minus the initial dark-adapted S_1 state) obtained from monomeric PSIIcc of *S. elongatus* after incubation with NO• at −30 °C overnight. Because of the frailness of the *S. elongatus* PSII core samples in the presence of NO•, the spectra that are shown were obtained prior to NO• removal (see Materials and Methods). Therefore, they also contain the free NO• EPR signal which is centered at $g = 2$ (see ref *49*). For clarity of presentation, most of this signal has been cut out, but the initial increase in the baseline on the high-field side is still caused by NO•.

For comparison, the S_{-2} EPR signal from spinach PSII membranes is shown in Figure 1B. This signal was obtained under virtually identical conditions. The overall resemblance of the two EPR signals, namely, a similar number of hyperfine peaks and the same spectral width (see arrows), suggests that the new NO•-induced EPR signal in *S. elongatus* PSIIcc also originates from the S_{-2} state. This assignment is further substantiated by flash-induced oxygen evolution patterns presented below.

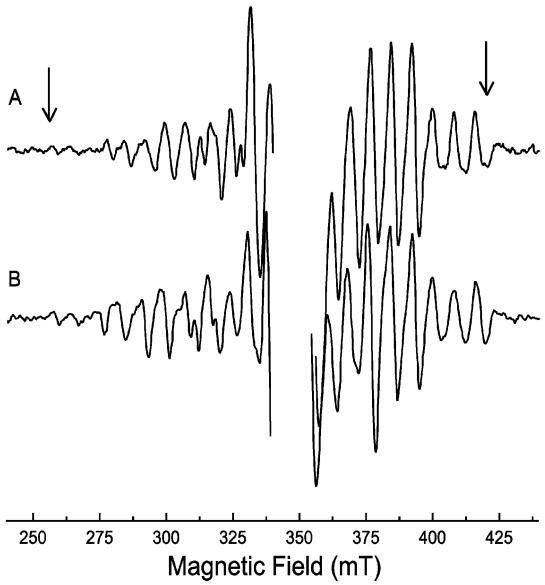

FIGURE 1: Comparison of S_{-2} EPR multiline signals (after subtraction of the S_1 dark-stable spectrum) of *S. elongatus* monomeric core complexes (A) and spinach PSII membranes (B). The arrows indicate the spectral width of the complete spectrum which is identical in both cases. The central part of the spectra, which is distorted by the signal of free NO•, was removed for clarity. EPR conditions: $T = 8.5$ K, microwave frequency of 9.64 GHz, microwave power of 31 mW, and modulation amplitude of 20 G.

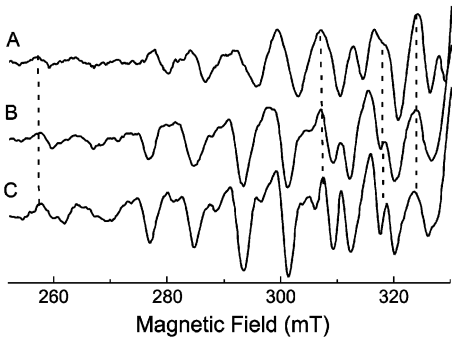

FIGURE 2: Comparison of the low-field part of the S_{-2} EPR multiline signal: (A) *S. elongatus* monomeric core particles, (B) spinach PSII membranes (H_2O), and (C) spinach PSII membranes (D_2O). Experimental conditions were as described in the legend of Figure 1.

In our initial attempts, we used glycerol instead of sucrose as a cryoprotectant in the buffer, because the PSIIcc are more stable in such a buffer. In such samples, NO• incubation did not generate a multiline signal, although parallel flash-induced oxygen evolution measurements on thylakoids showed that the samples were reduced also under these conditions (data not shown, but similar to those presented below). Similarly, our tests showed that the addition of alcohols (methanol or ethanol) affects primarily the EPR multiline signal amplitude and not S_{-2} state formation. In contrast, when mannitol was used, neither an EPR multiline signal nor a reduction was found.

Because of the excellent signal-to-noise ratio obtained for the S_{-2} state samples in sucrose buffer, a detailed comparison of the two EPR spectra is possible. Such an inspection (Figure 2, traces A and B) reveals that the hyperfine structures of the two S_{-2} state EPR signals are somewhat

Table 1: Approximate Center-to-Center Distances between Different Cofactors of the Dimeric PSIIcc from *S. elongatus*[a]

cofactors	approximate distance (Å)	cofactors	approximate distance (Å)
Mn_4(a)−Mn_4(b)	80	Mn_4(a)−cyt b_{559}(a)	55
Mn_4(a)−cyt c_{550}(a)	30	Mn_4(a)−cyt b_{559}(b)	110
Mn_4(a)−cyt c_{550}(b)	105		

[a] The numbers that are given are based on the 3.8 Å crystal structure (*31*). Labels a and b refer to the two PSII monomers of a dimeric PSIIcc.

different on the low-field side. In contrast, most peaks on the high-field side do line up. These differences have been consistently observed with several different PSIIcc samples. Thus, the spinach and *S. elongatus* S_{-2} EPR multiline spectra are very similar, but not identical. For an accurate quantification of the observed differences, measurements at other EPR frequencies or Mn ENDOR spectroscopy is required. This is beyond the scope of the current study.

To test the effect of proton hyperfine coupling on the structure of the S_{-2} state EPR signal, this signal was generated in a spinach sample suspended in D_2O buffer. The comparison of EPR traces B and C in Figure 2 shows that the hyperfine structure in the D_2O sample is better resolved than in the H_2O sample which results from line narrowing. The hyperfine peak positions remain, however, unchanged.

The question of whether there is a magnetic interaction between the two PSII units in a dimeric PSIIcc that influences the EPR signals of the Mn_4 cluster has been raised (*38*). To test this interesting hypothesis for the case of the S_{-2} EPR multiline signal, we have generated the S_{-2} state also in a dimeric PSIIcc isolated from *S. elongatus.* An S_{-2} EPR multiline signal identical to that of the monomers was found (data not shown). In the case of the S_{-2} state, this makes a magnetic interaction of the two OECs or of cytochrome c_{550} or b_{559} from monomer *a* with the OEC in monomer *b* in a dimeric PSIIcc unlikely. This result is in agreement with the distances between these components that can be obtained from the PSII crystal structure (Table 1). The distance between cytochrome c_{550} and the OEC within a monomer is ∼3 times shorter than that between the OEC and the cytochrome c_{550} of the attached monomer.

In addition to the reduction of the Mn_4 cluster, which leads to the S_{-2} state EPR multiline signal, NO• also binds to the non-heme iron on the acceptor side of PSII. This reversible binding of NO• to high-spin Fe^{2+} ($S = 2$) gives rise to an $S = {}^3/_2$ state (*49*). Following short NO• incubation, a $g = 4$ EPR signal from the Fe(II)−NO complex is formed. Under our experimental conditions, this signal is indistinguishable in spinach and *S. elongatus* (data not shown).

Flash-Induced Oxygen Evolution. Flash-induced oxygen evolution patterns can provide insight into the reaction pathways of exogenous reductants of the OEC, since they allow the analysis of the S state composition of the samples after various incubation times and/or after treatment with different reductant concentrations (see, for example, refs *27* and *48*). To avoid side reactions, NO• was largely removed from the samples prior to the polarographic measurements presented below (see Materials and Methods for details).

The flash-induced oxygen oscillation pattern of Figure 3a is typical for PSII membrane fragments in the absence of exogenous electron donors (see, for example, ref *57*). The first maximum of oxygen evolution occurs after the third flash, which indicates a high S_1 state population in the dark-adapted sample prior to flash illumination. At higher flash numbers, the oxygen yield decreases because the natural plastoquinone acceptor pool becomes reduced and thereby stable charge separation is prevented. Figure 3b shows that NO• incubation leads to a clear shift of the first maximum into the sixth flash. This measurement was obtained with an aliquot of a spinach PSII membrane sample that displayed an intense NO•-induced EPR multiline signal. The observed shift shows that NO• has reduced a large number of PSII centers into the S_{-2} state, which contains three additional electrons compared to the dark-stable S_1 state. For spinach PSII membranes, this finding confirms similar results from a recent study (*30*). The higher steady state oxygen yields observed after NO• incubation of the PSII membranes (Figure 3b) are indicative of the inactivation of part of the PSII complexes. The reason for this is that in the absence of exogenous electron acceptors the loss of some centers increases the number of available plastoquinone molecules for the PSII complexes that remain capable of oxygen evolution and share a common acceptor pool with the inactivated center(s) within a thylakoid membrane fragment. This effect has been previously observed using inhibitors such as DCMU (*58*). Because (i) no free Mn is observed in EPR measurements prior to the oxygen measurements and (ii) the S_{-2} state EPR signal has a very high intensity, this inactivation most likely occurs during the sample handling required to remove NO• before the oxygen measurements (see Materials and Methods for details).

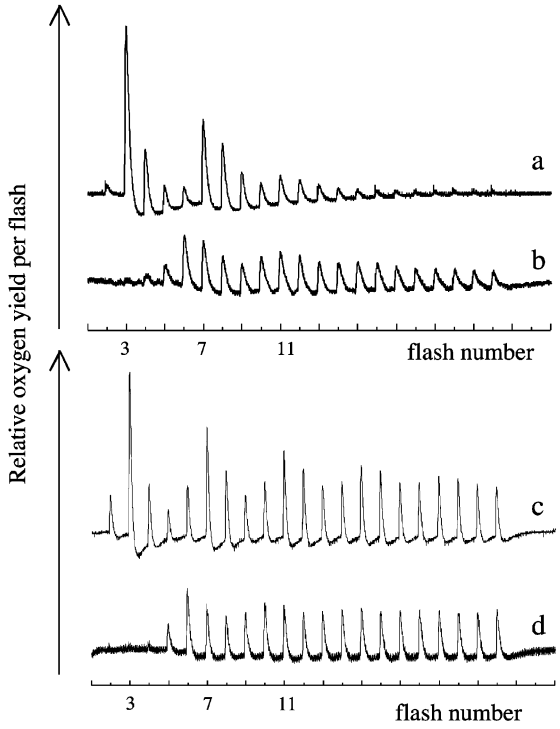

FIGURE 3: Flash-induced oxygen evolution patterns of spinach PSII membranes (a and b) and *S. elongatus* thylakoids (c and d) at 20 °C and pH 6.5. Traces a and c were obtained with untreated control samples, while traces b and d were obtained after incubation of the PSII samples with NO• at −30 °C overnight. In the latter cases, NO• was removed prior to the polarographic measurements (for details, see Materials and Methods). The flash frequency was 2 Hz. No exogenous electron acceptors were added.

Table 2: Fits of Oxygen Oscillation Patterns Shown in Figure 3[a]

							unknown donors									
fit	S_2 (%)	S_1 (%)	S_0 (%)	S_{-1} (%)	S_{-2} (%)	S_{-3} (%)	"S_{-4}" (%)	"S_{-5}" (%)	Y_D-NO (%)	α_{Y_D-NO} (%)	k_{21} (s^{-1})	k_{32} (s^{-1})	α (%)	β (%)	d	fq ($\times 10^{-6}$)
C1	−	100[b]	−	−	−	−	−	−	−	−	−	−	11.3	7.1	99.9	19
C2	7.2	77.8	9.2	5.8	−	−	−	−	−	−	−	−	8.7	4.9	99.0	1.7
C3	7.4	75.0	9.5	5.7	0.0	0.0	0.0	2.4	−	−	−	−	8.4	4.7	98.7	3
NO1	−	7.5	12.7	5.4	74.4	−	−	−	−	−	−	−	8.7[b]	4.9[b]	100[b]	248
NO2	−	1.0	0.2	15.3	83.6	−	−	−	−	−	−	−	18.1	4.9[b]	100[b]	34
NO3	−	0.4	0.0	26.0	73.7	−	−	−	87	76	−	−	8.7[b]	4.9[b]	99.7	36
NO4	−	0.0	6.7	23.0	70.3	−	−	−	53	−	14	14	8.7[b]	4.9[b]	100	68
NO5	−	1.1	0.0	8.1	49.7	19.7	20.2	1.2	−	−	−	−	8.7[b]	4.9[b]	99.2	8

[a] The extended Kok model described in Materials and Methods and the extensions outlined in the text and in the Supporting Information were used to fit the oxygen oscillation patterns of dark-adapted *S. elongatus* control thylakoids (fits C1−C3 and Figure 3c) and NO•-reduced thylakoids (fits NO1−NO5 and Figure 3d) under different conditions (see the text). The parameters are as follows: S_2−S_{-5}, normalized S state populations of the OEC [currently only preliminary evidence for the S_{-4} and S_{-5} states exists (*28*)]; Y_D-NO, nitrosotyrosine D which may act as an additional donor to $P680^+$ or the S_2 and S_3 states; α_{Y_D-NO}, miss factor for proposed $P680^+$ reduction by Y_D-NO; k_{21} and k_{32}, rate constants for possible reductions of the S_2 and S_3 states, respectively, by Y_D-NO (in fit NO4, only the lower limit is given); α, miss probability; β, double-hit probability; *d*, damping parameter; and fq, fit quality (see Materials and Methods). The first 16 flash-induced oxygen yields of each oscillation pattern have been analyzed. [b] Parameters fixed to the value given in the table. −, parameters excluded from fit.

Since we cannot use exogenous electron acceptors in our Joliot type oxygen electrode setup and PSIIcc are largely devoid of the natural quinones, we were not able to obtain analogous data for *S. elongatus* PSIIcc. To prove that in *S. elongatus* samples the S_{-2} state can also be populated by NO• incubation, we provide data using *S. elongatus* thylakoids (Figure 3c,d). Clearly, flash-induced oxygen oscillation patterns very similar to those shown above for spinach PSII membranes were obtained. The significantly higher steady state oxygen yields in *S. elongatus* thylakoids, which are not related to species but are due to the plastoquinone pool in thylakoids being larger than that in PSII membranes, allow a detailed analysis of these patterns in the framework of an extended Kok model (see Materials and Methods). Fits C1−C3 in Table 2 give normalized S state populations and the miss (α) and double-hit (β) probabilities calculated for the *S. elongates* thylakoid control measurement (Figure 3c). If a 100% S_1 state population is assumed, a reasonable fit was achieved with an α of 11.3% and a β of 7.1%. A significant improvement in fit quality is obtained when some S_2, S_0, and S_{-1} state populations are also allowed (fit C2). The small S_2 state population is due to incomplete dark adaptation after the preflash treatment employed to oxidize most of Y_D through back reactions with the S_2 state. No further improvement in fit quality resulted when the S_{-2}, S_{-3}, S_{-4}, and/or S_{-5} states were also included as free parameters (fit C3).

On the basis of EPR spectroscopy, the lowest S state reached by NO• incubation is the S_{-2} state. Therefore, we attempted to fit the pattern in Figure 3d (see fit NO1) by only varying the S_1−S_{-2} state populations and keeping the miss and double-hit probabilities fixed to the values found for the control in fit C2. While this type of fit approach gives excellent results with samples reduced by moderate concentrations of hydrazine or hydroxylamine (*48*), it obviously fails to fit the data presented in Figure 3d. If, in addition, the miss parameter is varied (fit NO2), a significantly better but still insufficient fit quality can be achieved with a very high miss factor of ∼18%. It is therefore worthwhile to consider the possibility that additional donors are formed during NO• incubation.

It was found recently (*24*) that NO• can slowly ($t_{1/2}$ = 20 h at −30 °C) react with Y_D^{ox} and form the EPR silent nitrosotyrosine (Y_D-NO). It is expected that Y_D-NO is a much more efficient electron donor then Y_D itself (*24*). Therefore, Y_D-NO formation might be able to explain the increased miss parameter of fit NO2 by either direct electron donation to $P680^+$ or rapid back reactions of the S_2 and S_3 states during the dark times between the flashes. To further analyze these two possibilities, the Kok model described in Materials and Methods was further extended to account for one additional donor (Y_D-NO) that can be oxidized only once within a flash train at the expense of the OEC. Fit NO3 shows that a fit quality similar to that of fit NO2 can be achieved if the initial Y_D-NO population is ∼85% and the miss probability α_{Y_D-NO} is ∼75%. However, on the basis of the reported half-time of ∼20 h at −30 °C for Y_D-NO formation (*24*), this value for the initial Y_D-NO population is significantly higher than one would expect to generate by an overnight incubation with NO•. It is therefore worthwhile also to consider back reactions of the S_2 and S_3 states with Y_D-NO during the dark times (t_d) of 0.5 s between the flashes. Fit NO4 represents the best fit achieved when in addition to the S_1−S_{-2} states only the fraction of Y_D-NO centers and the two rate constants k_{32} for the S_3Y_D-NO → S_2Y_D-NO^{ox} reaction and k_{21} for the S_2Y_D-NO → S_1Y_D-NO^{ox} reaction were varied (for details, see the Supporting Information). The fit quality of this fit (NO4) is worse by a factor of 2 compared to fits NO2 and NO3. Therefore, fits NO2−NO4 show that Y_D-NO formation alone is unable to fully explain the observed shifts in Figure 3d.

As additional "unknown" donors, S states below the level of the S_{-2} state may be considered. Recent studies using hydrazine or hydroxylamine as the reductant have provided clear evidence that reduced PSII samples can attain a fairly stable S_{-3} state (*27*). In addition, first indications for the S_{-4} and S_{-5} states have been presented (*28*). The S_{-5} state would represent the lowest possible oxidation state of the OEC [i.e., $Mn(II_4)$] if (i) the oxidation states of the S_1 state are Mn_4(III, III, IV, IV) as commonly assumed (*1*−*3*, *19*; see, however, ref *33*) and (ii) only Mn-centered reductions take place. Although at present no EPR-based evidence exists that states below the S_{-2} state can be generated by NO• treatment at −30 °C, we are not aware of any principle reasons why NO• should not be able to act in a manner similar to that of

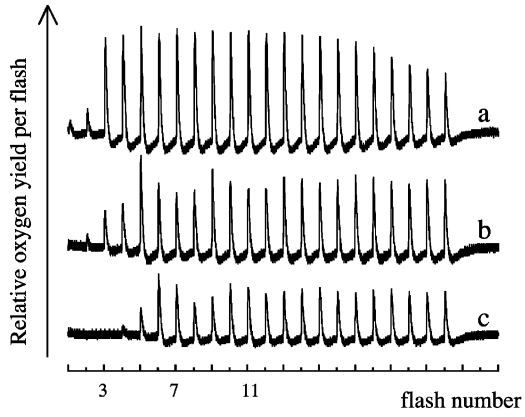

FIGURE 4: Flash-induced oxygen evolution patterns of *S. elongatus* thylakoids at 20 °C and pH 6.5 after incubation of PSII samples with NO• on ice for various times: (a) 20 min, (b) 1 h, and (c) 4 h. The flash frequency was 2 Hz. NO• was removed before the polarographic measurements. No exogenous electron donors were added.

other reductants and form small fractions of states below S_{-2}. In fact, the case of di-Mn-catalase from *Thermus thermophilus* shows that NO• can reduce Mn ions down to the Mn(II)Mn(II) level (*50*). This possibility has been analyzed in fit NO5, in which the S_1-S_{-5} state populations were varied, but the miss and double-hit probabilities were fixed to the control values. This fit approach gave an excellent fit quality, which is comparable to that of fit C2 of the control.

Although EPR measurements on similar samples show no indications for residual NO• after our NO• removal procedure, we cannot fully exclude the possibility that a small fraction of NO• is bound to the OEC in an EPR silent form. Accordingly, at present the possibility that the unknown donors in Table 2 may also represent bound NO•-donating electrons during the flash train cannot be excluded. In contrast, a direct contribution of NO• or its possible photo-induced derivatives to the polarographic signals can be ruled out on the basis of the absence of any flash-induced signals during the first three flashes in Figure 3d.

It is intriguing that the S_{-2} EPR signal is only observed when the NO• reduction is performed at approximately −30 °C. Furthermore, when a sample displaying the S_{-2} EPR multiline signal is warmed to 0 °C and is then quickly frozen to liquid nitrogen temperatures without a short incubation at −30 °C, then the S_{-2} EPR multiline signal is lost (*24*). To test whether the incubation of the OEC with NO• at ice temperatures nevertheless also leads to the formation of the S_{-2} state and to learn more about the reduction mechanism, we incubated *S. elongatus* thylakoids with NO• for various times on ice. Then the NO• was removed, and flash-induced oxygen evolution patterns were measured. The data in Figure 4 reveal that also at ice temperatures a reduction of the Mn_4 cluster in one-electron steps of the type $S_1 \rightarrow S_0 \rightarrow S_{-1} \rightarrow S_{-2}$ ($\rightarrow S_{-3}$) takes place. This can be seen by the stepwise shift of the first maximum of oxygen evolution from the third through the fourth and fifth flashes to the sixth flash. Interestingly, although the magnitude of the fourth flash undoubtedly increases transiently at short incubation times (Figure 4a), no circumstances were found where it was clearly the maximum. This indicates that, like the reduction of the OEC with hydroxylamine (*48*), the S_0 state reacts slightly faster with NO• than the S_1 state (see also ref *26*).

DISCUSSION

Flash-Induced Oxygen Evolution. A qualitative inspection of the flash-induced oxygen evolution patterns obtained in this study reveals that the OEC is reduced by NO• at −30 °C (Figure 3a,b) to states below S_0. The occurrence of the first maximum of oxygen evolution in the sixth flash suggests that most centers are in the S_{-2} state. In the case of spinach PSII membranes, the measurement of flash-induced oxygen yields could be performed on a sample that was first measured by EPR and displayed an intense NO•-induced multiline signal. These results confirm therefore the earlier assignment of the NO•-induced multiline signal from spinach samples to the S_{-2} state (*30*).

Because no exogenous electron acceptors can be used in our polarographic measurements, such a direct comparison between EPR and polarographic measurements proved to be impossible for the case of PSIIcc from *S. elongatus*. However, the new NO•-induced EPR signal in these *S. elongatus* samples can also be assigned to the S_{-2} state on the basis of (i) the great similarity of the S_{-2} EPR spectrum of the spinach sample (Figures 1 and 2; see below) and (ii) the shift of the first maximum to the sixth flash in flash-induced oxygen yield patterns obtained from *S. elongatus* thylakoids after NO• incubation under similar conditions (Figure 3d).

The large plastoquinone pool of thylakoids allows a detailed analysis of the NO-induced flash patterns within extended Kok models (see Table 2). Since many different effects may contribute to the observed shifts of the flash-induced oxygen yields to higher flash numbers, different fit approaches have been applied. These consider effects such as (i) a direct electron donation from Y_D-NO to $P680^+$, (ii) electron donation from Y_D-NO to the S_2 and S_3 states, and (iii) the population of S states below the level of the S_{-2} state. With the current data, it is impossible to decide which of the fits (NO3, NO4, or NO5) is closest to reality. Probably all three effects contribute to the observed patterns. Nevertheless, the fits clearly show that 50−75% of the PSII centers are in the S_{-2} state after NO incubation at −30 °C overnight. This demonstrates that NO• can also convert the OEC of *S. elongatus* into the S_{-2} state and supports thereby the assignment of the new EPR signal to this state. However, clearly a mixture of states is present in our samples with additional contributions from the S_{-1} state and, possibly, also from states below S_{-2}. Further studies are required to support the latter result.

EPR. Like the S_2 state of the "normal" Kok cycle, the reduced S_{-2} state gives rise to a strong EPR signal which provides valuable information about the electronic structure of the manganese cluster. The conditions for obtaining the S_{-2} EPR multiline signal are more critical than those required to observe the S_2 state EPR multiline signal. Incubation temperatures different from −30 °C (under our conditions approximately ±5 °C), the use of different cryoprotectants (vide supra), and the addition of alcohols (*24*, *26*, *30*) all prevent the observation of this signal, although in many cases the formation of the S_{-2} state takes place as deduced from flash-induced oxygen yield measurements (ref *30* and this study). For example, reduction at 0 °C (Figure 4) does not lead to the EPR "active" S_{-2} state (data not shown). The reasons for this specific temperature dependence of the

magnetic properties of the Mn_4 cluster are not yet understood.

The fact that the delicate S_{-2} state EPR signal can be generated in *S. elongatus* under virtually identical conditions as in spinach samples provides further evidence for the overall similarity of the OEC in plants and cyanobacteria (*17*, *37*−*40*). The small but reproducible differences observed in the hyperfine structure between the S_{-2} EPR multiline signal from spinach and *S. elongatus* PSIIcc are, however, indicative of minor structural differences in the coordination geometry and/or the ligands of the Mn_4 clusters.

Although the OEC contains four Mn ions, spectral simulations of the S_{-2} state EPR multiline signal from spinach PSII membranes showed that this signal can be ascribed to a magnetically isolated Mn_2(II, III) dimer (*25*). This result for the S_{-2} state may be rationalized within an Mn_4 cluster by a magnetic coupling of the four Mn ions to the limit of two uncoupled dimers (*33*). The reasons why the four Mn ions do not interact magnetically in a similar way as for example in the S_2 state, where a coupling between all four Mn ions is assumed (for a review, see ref *34*), are not understood. Protonation and loss of μ-oxo bridges during the reduction of the Mn_4 cluster are possible explanations (see also refs *25* and *51*).

To better understand how incubation at −30 °C leads to a magnetic isolation of the $NO^{\bullet}$-induced Mn_2(II, III) dimer within the tetranuclear OEC, it would be very helpful to identify the two of the four Mn ions that give rise to the observed EPR multiline signal. On the basis of the overall spectral similarity, it can be concluded that the same Mn_2(II, III) dimer gives rise to the S_{-2} EPR multiline signal in both spinach and *S. elongatus* samples. In the following, we can therefore combine structural information obtained by EXAFS and EPR spectroscopy with spinach PSII and those gathered from crystallography on *S. elongatus* samples.

Interestingly, the simulation parameters of the S_{-2} EPR multiline signals are very similar to those of the EPR signal of dimanganese catalase in the Mn_2(II, III) form (*25*, *52*). This may indicate a structural resemblance of the active center of Mn catalase in redox state Mn_2(II, III) and the dimeric building block of the OEC that gives rise to the S_{-2} EPR signal. The crystal structure of Mn catalase in *T. thermophilus* shows that the Mn−Mn distances are 3.18 Å in the Mn_2(II, II) form and 3.14 Å in the Mn_2(III, III) form and that in the fully reduced form the two Mn ions are bridged by one hydroxide, one water, and one carboxylate (*53*). This bridging motif of the Mn_2(II, II) dimer is similar to suggested bridging ligands of the 3.3 Å Mn−Mn distance in the OEC (*3*).

Additional information about the two Mn ions of the Mn_4 cluster that give rise to the S_{-2} EPR multiline signal comes from the orientation dependence of this signal. A study with partially oriented spinach samples suggested that the Mn−(μ-oxo)−Mn plane makes an angle of ∼20 with the membrane plane (*51*). This can be compared to Mn−Mn vectors determined by EXAFS spectroscopy. On the basis of new data for the Mn−Ca(Sr) vector (*54*), the orientation dependence of the 3.3 Å peak in Mn EXAFS could be deconvoluted into the Mn−Ca and Mn−Mn vectors at 3.4 and 3.3 Å, respectively (*36*). This deconvolution results in an angle of ∼28° for the 3.3 Å Mn−Mn vector relative to the membrane plane. On the basis of these results, we propose that the Mn_2(II, III) dimer of the S_{-2} state might be assigned to the two Mn ions which form the 3.3 Å vector determined by EXAFS spectroscopy of PSII in the physiological S states.

From the 3.8 Å PSII crystal structure (*31*), the four shortest Mn−Mn vectors can be estimated to lie approximately 0, 25, 25, and 60° off the membrane plane. At 3.8 Å resolution, it is impossible to discern exact Mn−Mn distances from the X-ray structure, but the four distances are all around 3 Å. Therefore, they probably correspond to the three 2.7 Å Mn−Mn distances and the one 3.3 Å Mn−Mn distance deduced from EXAFS spectroscopy in the S_0 state (55). The crystallographic data show that there are two Mn−Mn vectors in the OEC with an angle similar to that determined by EPR for the Mn−Mn pair giving rise to the S_{-2} state multiline signal and to that obtained from EXAFS for the 3.3 Å Mn−Mn vector. Therefore, a definitive assignment of the 3.3 Å Mn−Mn vector and, thereby, a possible identification of the two Mn ions forming the S_{-2} multiline cannot be achieved at present. Alternatively, as suggested previously (*51*), the one 2.7 Å Mn−Mn distance of the OEC that has an appropriate angle for the S_{-2} state EPR signal might become elongated to ∼3.0−3.3 Å during the reduction process. A further discussion has to await a higher-resolution crystal structure of PSII, EXAFS studies of the S_{-2} state, and detailed EPR studies on synthetic Mn_2(II, III) complexes with different bridging motifs.

In conclusion, we were able to show that the S_{-2} state EPR signal can be generated in cyanobacteria in a manner similar to that in plants. Its signal magnitude and simple hyperfine structure make it ideal for a comparison between different oxygen-evolving species and may allow the application of advanced EPR techniques in the future.

ACKNOWLEDGMENT

We thank D. DiFiore (TU Berlin) for excellent technical assistance during isolation of the PSII samples from *S. elongatus* and K.-O. Schäfer (TU Berlin) and Dr. V. Petrouleas (Institute of Material Sciences, NCSR "Democritos") for helpful discussions and critically reading the manuscript.

SUPPORTING INFORMATION AVAILABLE

Extensions to the Kok model to account for a possible direct electron donation from Y_D-NO to $P680^+$ or the S2 and S3 states. This material is available free of charge via the Internet at http://pubs.acs.org.

REFERENCES

1. Debus, R. J. (1992) *Biochim. Biophys. Acta 1102*, 269−352.
2. Britt, R. D. (1996) in *Oxygenic Photosynthesis: The Light Reactions* (Ort, D. R., and Yocum, C. F., Eds.) pp 137−164, Kluwer Academic Publishers, Dordrecht, The Netherlands.
3. Yachandra, V. K., Sauer, K., and Klein, M. P. (1996) *Chem. Rev. 96*, 2927−2950.
4. Kok, B., Forbush, B., and McGloin, M. (1970) *Photochem. Photobiol. 11*, 457−476.
5. Dismukes, G. C., and Siderer, Y. (1981) *Proc. Natl. Acad. Sci. U.S.A. 78*, 274−278.
6. Messinger, J., Robblee, J. H., Yu, W. O., Sauer, K., Yachandra, V. K., and Klein, M. P. (1997) *J. Am. Chem. Soc. 119*, 11349−11350.
7. Messinger, J., Nugent, J. H. A., and Evans, M. C. W. (1997) *Biochemistry 36*, 11055−11060.

8. Åhrling, K. A., Peterson, S., and Styring, S. (1997) *Biochemistry 36*, 13148−13152.
9. Casey, J. L., and Sauer, K. (1984) *Biochim. Biophys. Acta 767*, 21−28.
10. Zimmermann, J.-L., and Rutherford, A. W. (1984) *Biochim. Biophys. Acta 767*, 160−167.
11. Boussac, A., Un, S., Horner, O., and Rutherford, A. W. (1998) *Biochemistry 37*, 4001−4007.
12. Dexheimer, S. L., and Klein, M. P. (1992) *J. Am. Chem. Soc. 114*, 2821−2826.
13. Yamauchi, T., Mino, H., Matsukawa, T., Kawamori, A., and Ono, T.-a. (1997) *Biochemistry 36*, 7520−7526.
14. Campbell, K. A., Peloquin, J. M., Pham, D. P., Debus, R. J., and Britt, R. D. (1998) *J. Am. Chem. Soc. 120*, 447−448.
15. Matsukawa, T., Mino, H., Yoneda, D., and Kawamori, A. (1999) *Biochemistry 38*, 4072−4077.
16. Ioannidis, N., and Petrouleas, V. (2000) *Biochemistry 39*, 5246−5254.
17. Boussac, A., Sugiura, M., Inoue, Y., and Rutherford, A. W. (2000) *Biochemistry 39*, 13788−13799.
18. Iuzzolino, L., Dittmer, J., Dörner, W., Meyer-Klaucke, W., and Dau, H. (1998) *Biochemistry 37*, 17112−17119.
19. Messinger, J., Robblee, J. H., Bergmann, U., Fernandez, C., Glatzel, P., Visser, H., Cinco, R. M., McFarlane, K. L., Bellacchio, E., Pizarro, S. A., Cramer, S. P., Sauer, K., Klein, M. P., and Yachandra, V. K. (2001) *J. Am. Chem. Soc. 123*, 7804−7820.
20. Bouges, B. (1971) *Biochim. Biophys. Acta 936*, 228−235.
21. Kok, B., and Velthuys, B. R. (1977) in *Research in Photobiology* (Castellani, A., Ed.) pp 111−119, Plenum Press, New York.
22. Velthuys, B., and Kok, B. (1978) *Biochim. Biophys. Acta 502*, 211−221.
23. Sivaraja, M., Hunziker, D., and Dismukes, G. C. (1988) *Biochim. Biophys. Acta 936*, 228−235.
24. Goussias, C., Ioannidis, N., and Petrouleas, V. (1997) *Biochemistry 36*, 9261−9266.
25. Sarrou, J., Ioannidis, N., Deligiannakis, Y., and Petrouleas, V. (1998) *Biochemistry 37*, 3581−3587.
26. Ioannidis, N., Sarrou, J., Schansker, G., and Petrouleas, V. (1998) *Biochemistry 37*, 16445−16451.
27. Messinger, J., Seaton, G., Wydrzynski, T., Wacker, U., and Renger, G. (1997) *Biochemistry 36*, 6862−6873.
28. Messinger, J., Robblee, J., Bergmann, U., Fernandez, C., Glatzel, P., Isgandarova, S., Hanssum, B., Renger, G., Cramer, S., Sauer, K., and Yachandra, V. (2001) in *12th International Congress on Photosynthesis*, pp S10−019, CSIRO Publishing, Collingwood, Australia.
29. Zheng, M., and Dismukes, G. C. (1996) *Inorg. Chem. 35*, 3307−3319.
30. Schansker, G., Goussias, C., Petrouleas, V., and Rutherford, A. W. (2002) *Biochemistry 41*, 3057−3064.
31. Zouni, A., Witt, H. T., Kern, J., Fromme, P., Krauss, N., Saenger, W., and Orth, P. (2001) *Nature 409*, 739−743.
32. Zouni, A., Kern, J., Loll, B., Fromme, P., Witt, H. T., Orth, P., Krauss, N., Saenger, W., and Biesiadka, J. (2001) in *12th International Congress on Photosynthesis*, pp S05−003, CSIRO Publishers, Collingwood, Australia.
33. Carell, T. G., Tyryshkin, A. M., and Dismukes, G. C. (2002) *J. Biol. Inorg. Chem. 7*, 2−22.
34. Peloquin, J. M., and Britt, R. D. (2001) *Biochim. Biophys. Acta 1503*, 96−111.
35. Renger, G. (2001) *Biochim. Biophys. Acta 1503*, 210−228.
36. Robblee, J. H., Cinco, R. M., and Yachandra, V. K. (2001) *Biochim. Biophys. Acta 1503*, 7−23.
37. McDermott, A. E., Yachandra, V. K., Guiles, R. D., Cole, J. L., Dexheimer, S. L., Britt, R. D., Sauer, K., and Klein, M. P. (1988) *Biochemistry 27*, 4021−4031.
38. Boussac, A., Kuhl, H., Ghibaudi, E., Rögner, M., and Rutherford, A. W. (1999) *Biochemistry 38*, 11942−11948.
39. Koike, H., Hanssum, B., Inoue, Y., and Renger, G. (1987) *Biochim. Biophys. Acta 893*, 524−533.
40. Renger, G., and Hanssum, B. (1992) *FEBS Lett. 299*, 28−32.
41. Boussac, A., Kuhl, H., Un, S., Rögner, M., and Rutherford, A. W. (1998) *Biochemistry 37*, 8995−9000.
42. Schatz, G. H., and Witt, H. T. (1984) *Photobiochem. Photobiophys. 7*, 1−14.
43. Zouni, A., Lüneberg, C., Fromme, P., Schubert, W. D., Saenger, W., and Witt, H. T. (1998) in *Photosynthesis: Mechanisms and Effects* (Garab, G., Ed.) pp 925−928, Kluwer Academic Publishers, Dordrecht, The Netherlands.
44. Berthold, D. A., Babcock, G. T., and Yocum, C. F. (1981) *FEBS Lett. 134*, 231−234.
45. Ford, R. C., and Evans, M. C. W. (1983) *FEBS Lett. 160*, 159−164.
46. Joliot, P. (1972) *Methods Enzymol. 24B*, 123−134.
47. Messinger, J. (1993) Ph.D. Thesis, Fachbereich 6, TU Berlin, Berlin, Germany.
48. Messinger, J., Wacker, U., and Renger, G. (1991) *Biochemistry 30*, 7852−7862.
49. Petrouleas, V., and Diner, B. A. (1990) *Biochim. Biophys. Acta 1015*, 131−140.
50. Ioannidis, N., Schansker, G., Barynin, V. V., and Petrouleas, V. (2000) *J. Biol. Inorg. Chem. 5*, 354−363.
51. Hanley, J., Sarrou, J., and Petrouleas, V. (2000) *Biochemistry 39*, 15441−15445.
52. Zheng, M., Khangulov, S. V., Dismukes, G. C., and Barynin, V. V. (1994) *Inorg. Chem. 33*, 382−387.
53. Barynin, V. V., Hempstead, P. D., Vagin, A. A., Antonyuk, S. V., Melik-Adamyan, W. R., Lamzin, V. S., Harrison, P. M., and Artymiuk, P. J. (1997) *J. Inorg. Biochem. 67*, 196.
54. Cinco, R. M., Fernandez, C., Messinger, J., Robblee, J. H., Visser, H., McFarlane, K. L., Bergmann, U., Glatzel, P., Cramer, S. P., Sauer, K., Klein, M. P., and Yachandra, V. K. (1998) in *Photosynthesis: Mechanisms and Effects* (Garab, G., Ed.) pp 1273−1278, Kluwer Academic Publishers, Dordrecht, The Netherlands.
55. Robblee, J. H., Messinger, J., Cinco, R. M., McFarlane, K. L., Fernandez, C., Pizarro, S. A., Sauer, K., and Yachandra, V. K. (2002) *J. Am. Chem. Soc. 124*, 7459−7471.
56. Shinkarev, V. P., and Wraight, C. A. (1993) *Proc. Natl. Acad. Sci. U.S.A. 90*, 1834−1838.
57. Messinger, J., Schröder, W. P., and Renger, G. (1993) *Biochemistry 32*, 7658−7668.
58. Renger, G., Messinger, J., and Fromme, R. (1989) *Z. Naturforsch. 44c*, 423−430.

BI026327P